International Journal of Aviation, Aeronautics, and Aerospace

Volume 9 | Issue 1 Article 6

2022

Heat Generation of Aircraft Tires at Landing

Yu Li
University of Sussex, yl697@sussex.ac.uk
Dr. Weiji Wang
University of Sussex, w.j.wang@sussex.ac.uk

Heat Generation of Aircraft Tires at Landing

Cover Page Footnote

Not applicable.

Aircraft wheels are free but still static after being extended from the fuselage because the oncoming high-speed airflow cannot spin them due to the symmetrical wheel geometry (Alroqi, 2017). Therefore, the wheels will skid and speed up on the runway to match the high aircraft speed. The friction can generate a large amount of heat, which raises the tire temperature, and leads to material decomposition and smokes.

The International Institute of Synthetic Rubber Producers (1999) states that the primary materials used to produce vehicle tire tread are Butadiene Rubber (BR) and Styrene-Butadiene rubber (SBR). However, these materials contain shortcoming in heat resistance, a significant ability demanded at landing friction. Some studies state that the critical temperature of BR is only at 425 K or 151.8°C (Majer & Svoboda, 1985; Tsonopoulos & Ambrose, 1996). Nonetheless, a USAF study says the peak temperature on an F-16 tire tread at landing is approximately 500ºF, or 260ºC (Zakrajsek et al., 2016). Undoubtedly, a standard BR tire cannot be used to combat the landing heat. On the other hand, natural rubber (NR) is selected as the primary material for the aircraft tire because of its high heat resistance (Grosch, 1969).

The NR tire surface is usually composed of a rubber coating rich in nylon. The addition of nylon can improve tire performance by giving its shape and strength. However, its physical characterization will still be affected by high temperatures. Early reports show that the critical temperature of the NR tire is at approximately 200°C (Dawson & Porritt, 1935Saibel & Tsai, 1973) and describe the tire tensile performance as temperature increases (Goodyear, 2020). Initially, the tire strength and adhesion start to reduce at 25°C or 77°F. The reduction becomes much more visible when the rubber reverts to the uncured state at around 140-160°C. Then, nylon starts to melt at 200°C, and the tire tensile drops to 50% of the original level. Finally, the tire loses its strength entirely at about 240°C or 464°F. It can be seen that the strength curve falls significantly when the temperature exceeds the melting point at 200°C as shown in Figure 1.

Figure 1

The Tensile of NR Tire Versus Temperatures

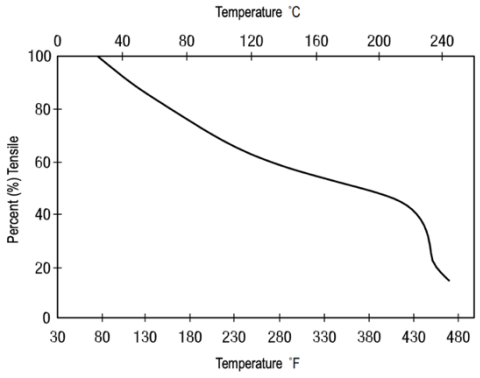

Consequently, 200°C is determined as the critical temperature of the tire surface material in this study. If the environment temperature is assumed 20°C,

the temperature rise will only need to exceed 180°C for the polymer decomposition to occur. Once reaching the critical temperature, approximately 50% to 90% of rubber particles will evaporate in white smoke, while the rest is cooled on the runway as black marks (Bennett et al., 2011).

There are several disadvantages of tire material decomposition. First, its environmental influence should be considered because of its non-degradable characteristic (Clark, 2013). The white smoke with deposited rubber contains hazardous chemical materials. An analysis of aircraft tire rubber waste supports more chemical composition with high agglomeration than car tire rubber (Adathodi et al., 2018). The analysis has tested different compositions of Silicon Oxide (17.61%), Molybdenum Oxide (7.61%), and many other oxides. Inhalation of crystalline silica oxide dust may cause silicosis, bronchitis, or cancer (Merget et al., 2002). On the other hand, the worn tire impacts aircraft performance and can even lead to accidents. In 2004, a Boeing 737-300 took off from Glasgow Airport. The left inboard tire shed its tread, which led to several hydraulic system contents loss, and the landing gear retracting mechanism was also damaged. The CAA accident report indicates that the damaged tire was close to its wear limit and the material fatigue also boosted the shedding (CAA, 2004). A typical solution to address tire wear in the current aviation field is conducting regular inspection and tire replacement at a high cost.

The tire tread temperature is flexible and depends on aircraft, landing environment and weather. Additionally, the measurement of tire temperature becomes a difficult task due to the very dynamic nature of friction. One study records a smoke generation that lasts for 0.32 seconds at most (Bennett et al., 2011), and another research also shows less than 0.5 seconds (Alroqi et al., 2016). The tire temperature will then drop rapidly due to the high-speed wheel rotation and airflow convection. As a result, it is more appropriate to develop a mathematical model to simulate the tire landing dynamic and temperature rise. The model can be used to indicate the tire wear level and help develop wear prevention technology. Three specific objects of study are also established as follows.

Tire Temperature on Different Categories of Aircraft

Since the 1940s, many attempts have been applied to solve the tire wear problem on wide-body aircraft, such as the Boeing 747 (Alroqi, 2017) and the Lockheed Constitution (Keyser, 1948). The great tire load and landing speed contribute to robust friction indeed. However, some evidence based on the black tire mark points out that tire wear also exists on light aircraft. See Figure 2.

Figure 2

The Video Screenshot of a DHC-6 Landing at Saint Barthélemy Airport

Note. Saint Barthélemy Airport which accepts general aviation aircraft like DHC-6 Twin otter at most. The black tire marks are visible especially on the white aiming key, the picture also shows the clear white smoke produced by tire friction (Watt, 2017).

Therefore, the first object of this study aims to determine how the heat generation on tire performs on different types of aircraft. Various types of aircraft are selected as research targets for a comprehensive comparison. Table 1 lists the targets with the required specifications.

Table 1

The Specifications of the Aircraft in this Study (Skybrary, 2021; Dunlop, 2021; Goodyear, 2002).

Aircraft	Embraer E-190	ATR 72	DHC 6
MLW	44,000 kg	22,400kg	5,580 kg
Landing speed	130 kt 67 m/s	110 kt 57 m/s	70 kt 36 m/s
Tire size	H41x16.0-20	H34x10.0-R16	11.0-12
Tire Width	0.41 m	0.25 m	0.28 m
Tire Radius	0.52 m	0.43 m	0.35 m
Tire Weight	70 kg	25 kg	18 kg

Tire Temperature Under Different Landing Weights

The second object is the influence of landing weight on tire temperature rise. Greater landing weight can boom the normal force and the friction on the tire. Thus, the thermal conduction on the tire could raise because of stronger friction. On the other hand, reducing tire load may decrease tire acceleration and extend speed up duration, which could also lead to greater thermal conduction. As a result, this study will adjust the aircraft landing weight to see the effect. ATR-72 is chosen with three landing weights as shown in Table 2.

Table 2

ATR-72 with Three Landing Weights

Aircraft	ATR-72
Maximum weight	22,400 kg
Median weight	17,700 kg
Minimum weight	13,000 kg

Note. The maximum weight is based on MLW and the minimum weight is based on the Operational Empty weight (OEW) (ATR, 2021). The data retains three significant figures.

Tire Temperature on Alternative Tire Selections

The manufacturer determines aircraft tires based on the flight performance. The third object is the friction performance under alternative tire configuration. For example, E-190 and E-190 E2 are "brother" aircraft with similar specifications, but Embraer equips different tires on them. This study will see whether it helps alleviate landing friction or aggravate this process if the default tire is changed. E-190 is taken as the research target, as shown in Table 3.

Table 3

The Official Tire Selection of Some Embraer Jets

Aircraft	Embraer E-190	Embraer E-190 E2	Embraer E-175
Tire size	H41x16.0-20	H42x16.0-20	H38x13.0-18
Tire Width	0.41 m	0.41 m	0.33 m
Tire Radius	0.52 m	0.53 m	0.48 m
Tire Weight	70 kg	60 kg	45 kg

Note. The official tire selection of some Embraer jets similar to E-190 (Dunlop, 2021; Goodyear, 2002), its tire will be replaced by the others to see the friction performance difference.

Before modelling and simulating the landing gear system, several assumptions are set to simplify the calculation and avoid meaningless analysis. In the first place, no wheel braking is applied after landing, and the aircraft speed remains constant. Secondly, the shock absorber has been removed despite an essential landing gear component. The stiffness and damping effects work on the entire system, which will violate the principle of variables control. Consequently, the tire contact surface or the tire patch remains constant in this study.

Finally, the aircraft main landing gears usually contact the runway first, followed by the nose gears. This time interval is much longer than the main landing gears speed up duration. Hence, the aircraft load is evenly distributed to the main landing gears only. Furthermore, only a proportion of the aircraft weight acts on the runway due to the lift effect, and the actual tire load is flexible depending on the angle of attack, landing speed, and even flap setting. The proportion is assumed 50% in this study, and further research on this area is demanded.

Modelling

A typical landing gear configuration on narrow-body aircraft contains two groups of main landing gears, each containing two wheels. According to the weight distribution assumption, the total wheel load is 50% of the Aircraft landing weight m_t and is evenly distributed to all the four wheels. As shown in Figure 3, the load of each wheel m_2 will be:

$$m_2 = 50\% \cdot \frac{1}{4} m_t = \frac{1}{8} m_t \quad (1)$$

Figure 3

The Layout of Landing Gear and Runway Surface

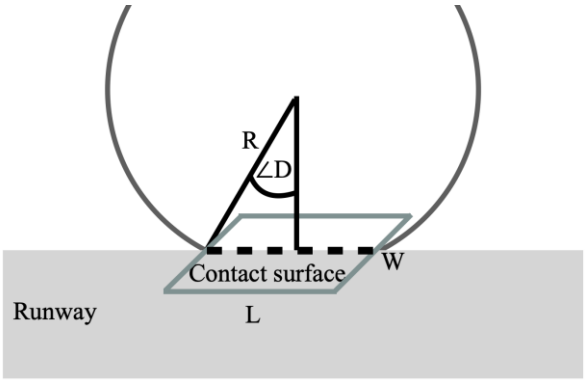

The wheel is simulated to speed up once it touches the runway, and the contact area remains unchanged due to the absence of shock absorber. Figure 3 depicts the basic layout of the entire system: The contact surface is assumed a rectangle with length *L* and width *W*, *∠D* is the semi-displaced angle of the contact surface, and it is supposed to be a constant because of a steady wheel radius *R*. In this study, this angle is assumed 0.3rad based on many observations on aircraft tires. Therefore, the length of the contact surface *L* will be:

$$\mathrm{L} = 2 \cdot R \cdot \sin 0.3 \quad (2)$$

The wheel normal force *Fn* is calculated in Equation 3 according to the wheel load *m2* and the wheel weight *m1*. Moreover, the friction *Fx* is the product of normal force *Fn* and friction coefficient μ. 0.7 is an appropriate coefficient for a rubber tire on a dry asphalt runway (Jones & Childers, 1993).

$$F_n = (m_1 + m_2)\, g \quad (3)$$

where $g = 9.81 m/s^2$

$$F_x = F_n \cdot \mu \quad (4)$$

where $\mu = 0.7$

According to the torque formula, it is possible to calculate the wheel angular acceleration α based on the wheel radius, wheel weight, and friction. The angular acceleration will be a constant as well.

$$\alpha = F_x/(m_1 \cdot R) \quad (5)$$

The acceleration duration T is obtained based on the angular acceleration in Equation 5 and the aircraft landing speed v. Also, the speed up distance in radians D is calculated in Equation 7:

$$T = \frac{v}{R\alpha} \tag{6}$$

$$D = \frac{1}{2}\alpha T^2 \tag{7}$$

The wheel angular speed v_a is the product of angular acceleration a and friction time t, and the wheel linear speed v_l is the product of angular speed and wheel radius. The wheel speed remains constant after acceleration completes.

$$v_a = \alpha t \tag{8}$$

$$v_l = v_a \cdot R \tag{9}$$

The temperature on the entire wheel circumference should be discussed, and a series of sampling points are evenly distributed. The total number of sampling points n_p with an interval of 0.1rad is calculated in Equation 10. Furthermore, the angle of each sampling point $\angle P_n$ is calculated in Equation 11, where n is the ordinal (n=1, 2, 3,…).

$$n_p = 10 \cdot D \tag{10}$$

$$\angle P_n = 0.1\,(n-1) \tag{11}$$

There will be overlapping sampling points if the wheel rotates more than one revolution in the acceleration. For example, the point $\angle P$ and the point $\angle P \pm 2\pi$. Therefore, those relevant results should be superimposed. This function can be achieved through the MATLAB programming.

The wheel speed builds evenly due to constant acceleration, and the speed difference between two sampling points is constant since all points are equidistant. Therefore, the friction speed of each sampling point follows an arithmetic sequence:

$$v_{f_n} = v - (n-1)\frac{v}{n_p} \tag{12}$$

Figure 4

A Sampling Point P with its Displaced Angle ∠P

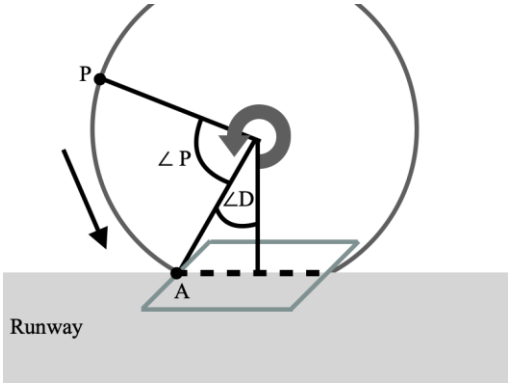

In addition, Figure 4 shows an example to calculate the friction duration of each sampling point. P is a randomly selected sampling point on wheel

circumference, and A is the border of the contact surface. When P has not entered the contact surface, the displaced angle $\angle P$ follows this rule:

$$\angle P = \frac{1}{2}\alpha {t_e}^2 \tag{13}$$

where t_e is the time to enter the contact surface.

On the other hand, the angle from the original position to the end of the contact surface is:

$$\angle P + 2 \cdot \angle D = \frac{1}{2}\alpha {t_l}^2 \tag{14}$$

where t_l is the time to leave the contact surface.

As a result, the entering t_e and leaving time t_l for any sampling points can be obtained by solving Equation 13 and 14 numerically and taking the non-negative value. Finally, the friction duration of a sampling point t_f will be:

$$t_f = t_l - t_e \tag{15}$$

The step after the tire dynamic modelling will be the heat transfer modelling. The essential step in this part is to divide the contact surface into identical rectangular elements for finite element analysis (FEA). Figure 5 shows the schematic diagram. The sampling point locates in the centre of the contact surface with position *(0, 0)*. The grey unit represents a single heat element with position *(x_e, y_e)*. See Figure 5. The coordinate on the z-axis is neglected since this study aims to work out the temperature on the tire surface.

Figure 5

The FEA Schematic Diagram

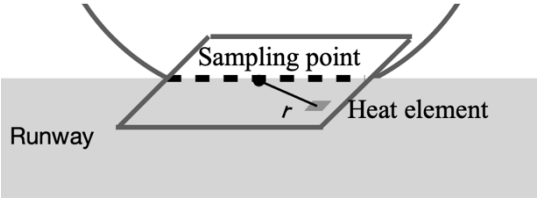

Note. Each heat element transmits thermal energy to the sampling point.

The core idea of the FEA is to calculate the thermal contribution of each element and accumulate them together. *r* is the distance between the sampling point and heat element, the square of *r* will be:

$$r^2 = x_e^2 + y_e^2 \tag{16}$$

Furthermore, the data of each element is filled into Laplace's heat equation to work out the temperature rise. The Laplace's heat equation has an initial format as follows (Bhushan, 2013).

$$\rho c \frac{\partial \theta}{\partial t} = k\left(\frac{\partial^2 \theta}{\partial x^2} + \frac{\partial^2 \theta}{\partial y^2} + \frac{\partial^2 \theta}{\partial z^2}\right) + \dot{\phi}(x, y, z, t) \tag{17}$$

$$\frac{\partial \theta}{\partial t} - a\left(\frac{\partial^2 \theta}{\partial x^2} + \frac{\partial^2 \theta}{\partial y^2} + \frac{\partial^2 \theta}{\partial z^2}\right) = f(x, y, z, t) \tag{18}$$

where

$a = k/(\rho c)$ $\quad \dot{\phi}(x, y, z, t) = \rho c \cdot f(x, y, z, t)$

The solution of Equation 18 will be

$$\theta = \frac{q}{\rho c(4\pi a)^{3/2}} \int_0^T \int_{-L/2}^{L/2} \int_{-W/2}^{W/2} \frac{e^{-r^2/4a(t-\tau)}}{(t-\tau)^{3/2}} dx_e dy_e d\tau \quad (19)$$

where q is the heat liberation rate of a heat element, T is the friction duration, τ is the time after the friction start, ρ is the density of rubber, c is the specific heat capacity and a is the thermal diffusivity (Kuo & Lin, 2006).

This solution includes an integral part, which calculates the heat contribution of each element and accumulates them in the form of integral over position and time. This integration has no analytical result and must be solved by numerical method. Additionally, the heat liberation rate of each element is the work of the friction energy divided by the number of heat elements n_e, and the rate will be halved to simulate the heat sharing by the runway. The side length of each element is 10^{-5} m and the area is 10^{-10} m^2.

$$q = \frac{1}{2} F_x \cdot (v - v_l)/n_e \quad (20)$$

Finally, Table 4 summarises the thermal properties of natural rubber.

Table 4

Thermal Properties of Natural Rubber

Properties	Value
Thermal conductivity k	0.15 W/m·K
Density ρ	1200 kg/m^3
Specific heat capacity c	2005 J/kg·K
Thermal diffusivity a	6.23×10^{-8} m^2/s

Result and Discussion

Tire Temperature on Different Categories of Aircraft

Figure 6 illustrates the linear wheel speed of all the three types of aircraft, and Table 5 lists the data of wheel speed up.

Figure 6
Aircraft Tires Linear Speed Change Versus Time

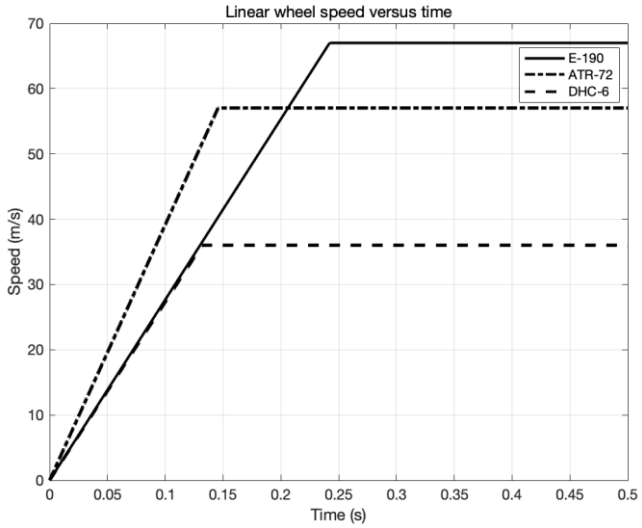

Table 5
Wheel Speed Up Data, The Speed Up Distance is Converted to Meters

Aircraft	Angular Acceleration	Linear Acceleration	Duration	Distance
E-190	532.0 rad/s^2	276.6 m/s^2	0.24 s	8.1 m
ATR-72	910.3 rad/s^2	391.4 m/s^2	0.14 s	2.4 m
DHC-6	779.9 rad/s^2	139.9 m/s^2	0.13 s	1.9 m

The acceleration of each wheel is obtained by Equation 5, in which the acceleration depends on friction, wheel weight and radius. Therefore, only a heavier wheel load is not adequate to guarantee a greater acceleration, but the wheel specification should also be considered. In this case, the angular acceleration of the DHC-6 wheel is even greater than that of E-190 because of very low wheel weight and radius values as the denominator. Moreover, the ATR-72 wheel experiences the greatest linear acceleration but it still takes a longer speed up duration than DHC-6 because of a higher target speed. Although the aircraft specifications differ, the average wheel friction duration is about 0.17 seconds, consistent with observations and research. The friction distance can also reflect the friction level: The distance of the E-190 wheel is about 8 meters, which is nearly four times that of DHC-6. It can be seen that the friction duration and distance are only related to the aircraft weight: Heavier aircraft will obviously lead to greater values, consistent with reality.

The tire surface temperature rises of three types of aircraft are plotted in Figure 7. The horizontal dotted line represents the material critical temperature, which is 180°C instead of 200°C because this figure shows the temperature rise

without including a 20°C environmental temperature. Any area of the tire circumference where the temperature value is above the dotted line will have material decomposition. See Figure 7.

Figure 7
The Temperature Rise on the Tire Circumference

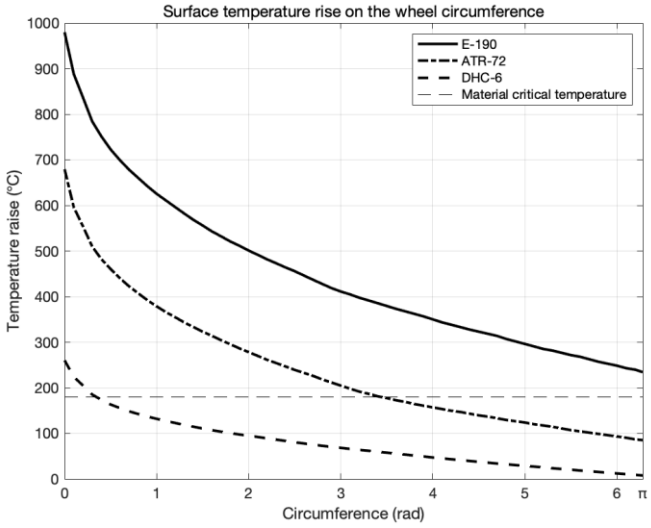

Table 8
The Maximum, Minimum, and Median Temperature Rises and the Decomposition Proportion on Each Tire

Aircraft	E-190	ATR-72	DHC-6
Maximum temperature rise	979.7°C	679.5°C	260.4°C
Minimum temperature rise	233.1°C	84.9°C	7.6°C
Median temperature	404.9°C	198.2°C	66.2°C
Decomposition Proportion	100%	55.7%	5.6%

Note. The median temperature is taken instead of the mean value because the influence of extreme values shall be avoided. The decomposition proportion indicates the percentage of the entire circumference where the material is decomposed.

The result shows significant differences of the tire temperature rise. First of all, the peak temperature of the E-190 tire is close to 1000°C, and the temperature rise of the entire tire circumference exceeds the critical value, which means the material decomposition occurs everywhere. Secondly, the tire of ATR-72 experiences a lower peak temperature of approximately 680°C because of reduced wheel load and friction speed. This time the decomposition proportion drops to 55.7%, and the temperature rise of the remaining circumference is below the critical value. In the third place, the temperature rise

of 94.4% of the DHC-6 tire circumference is kept below the critical value. In the last area of the circumference, the temperature rise is even close to zero. Nonetheless, the area that first contacts the runway still suffers from a material decomposition with a peak temperature of about 260°C. This point echoes the previous observations that general aviation aircraft like DHC-6 has tire-smoking at landing like large aircraft. Therefore, the decomposition of tire materials on this type of aircraft should also be paid attention to, as shown in Figure 8.

Figure 8

The Isotherm (pie chart) of Tire Temperature

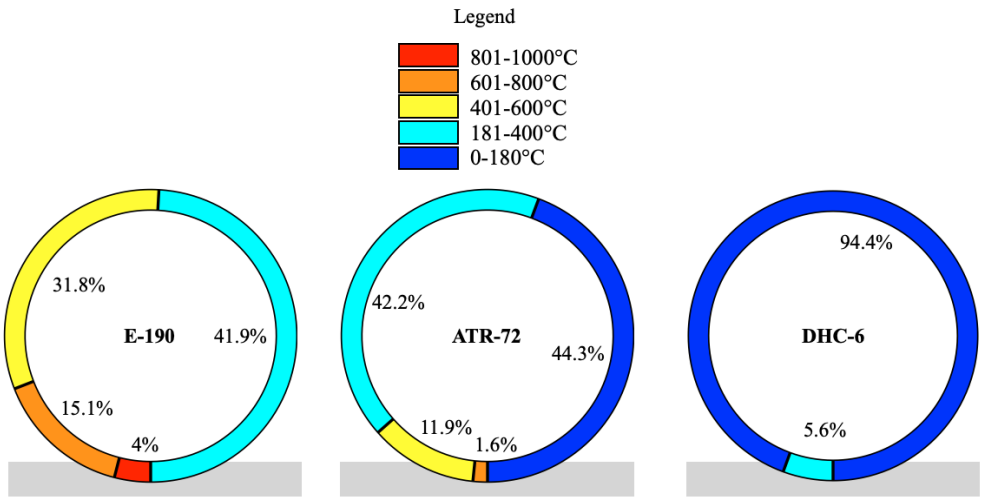

Note. Each wedge with different colour represents a temperature range, with red indicating the highest temperature and blue is the lowest. The grey rectangle represents runway. Wheel rotates anticlockwise.

The pie chart can reflect the temperature rise more intuitively. Among them, only the E-190 chart contains the red colour representing the highest temperature range, but it only accounts for 4% of the entire circumference. The percentage of the remaining temperature ranges increases successively, and the area with a temperature interval of 181°C - 400°C occupies almost half of the circumference. Secondly, the ATR-72 chart shows a blue colour representing the temperature below the critical point, and the non-material-decomposition area occupies nearly half of the circumference (44.3%). This time, no area on the tire surface exceeds 800°C, and only a tiny part exceeds 400°C (1.6%). Finally, the chart of DHC-6 is relatively simple because of its low-temperature rise. Only two wedges are contained, most of which are blue, indicating no material decomposition.

This part solved the first object and calculated the tire temperature of various types of aircraft. Large aircraft will inevitably lead to a higher friction temperature due to paramount weight and landing speed, but the same problem also occur on light aircraft.

Tire Temperature Under Different Landing Weights

The influence of aircraft weight on wheel speed up and heat generation is investigated in this part, the ATR-72 is chosen as the research target and its landing weight is modified. The results are shown in Figure 9.

Figure 9

The Average Friction Time and Speed of Each Sampling Point on the Tire Circumference Under Three Landing Weights

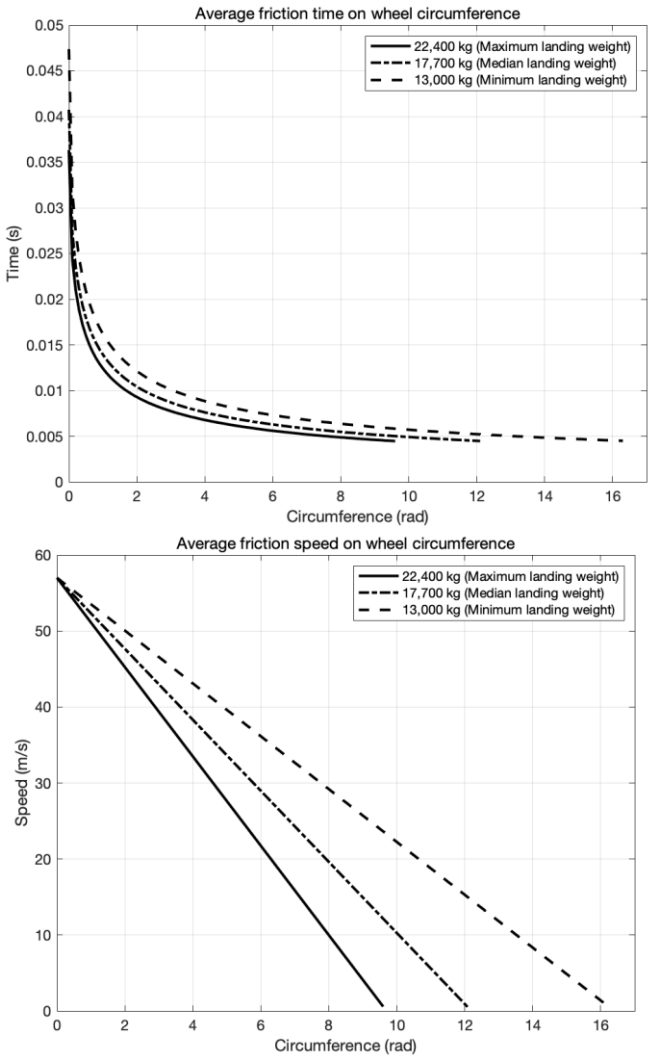

First of all, the friction duration of each sampling point is non-linear, manifested as a steep falling of the curve at 0rad and gradually flattening in the later part. Because the wheel is static when it touches the runway, and it takes a while for the sampling point to leave the contact surface. On the other hand, the gradient of speed curve is constant due to fixed acceleration. The later a sampling point starts friction, the higher the wheel speed and the lower the

friction speed at that moment. With the tire specification remaining unchanged, less landing weight leads to lower angular acceleration. Therefore, the wheel takes greater speed up time and distance, which could enhance the heat generation. See Figure 10 and Table 9.

Figure 10

The Temperature Rise Under Different Landing Weights

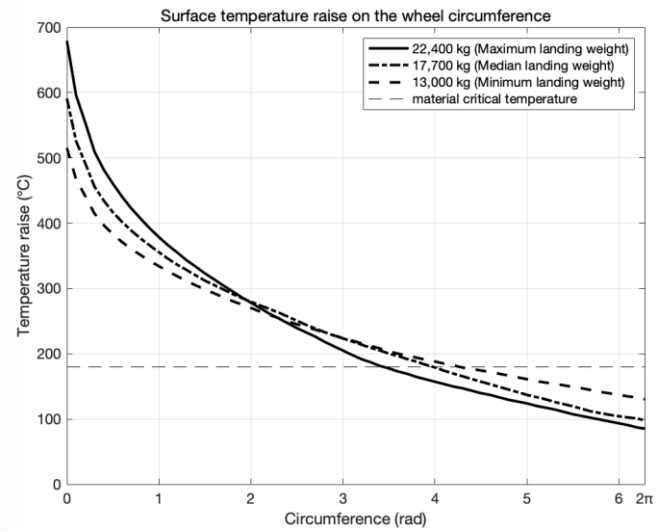

Table 9

The Friction Performance Under Different Landing Weights

Landing weight	Distance	Duration	Maximum temperature	Decomposition proportion
22,400 kg	2.4 m	0.14 s	679.5℃	55.7 %
17,700 kg	5.2 m	0.18 s	591.1℃	63.7 %
13,000 kg	7.1 m	0.25 s	515.4℃	68.5 %

It can be found that the temperature curves intersect in Figure 10. Although a heavier wheel load causes more robust friction and higher temperature rise in the first part of the circumference, it falls to the least. Table 9 discloses specific data: For the maximum landing weight, the wheel takes the shortest time and distance to speed up, and the peak temperature is close to 700°C with a decomposition proportion of 55.7%. On the other side, the peak temperature drops to around 500°C under minimum weight, but the decomposition proportion raises to 68.5% with longer speed up time and distance. The main factor could be the two-sided effects of landing weight on friction.

When friction starts, there is no significant difference in rotation speed. At this time, the strength of friction is mainly determined by the wheel load. An

increased load exerts greater friction on the tire, booming the heat transfer and temperature rise. In the later friction stage, the wheel under greater load completes friction early due to higher acceleration, while the lightly loaded wheel is still in the friction stage, increasing the friction temperature. Therefore, the impact of landing weight on tire temperature is manifold.

Tire Temperature of Alternative Tire Options

Figure 11

The Temperature Rise of Various Tire Options

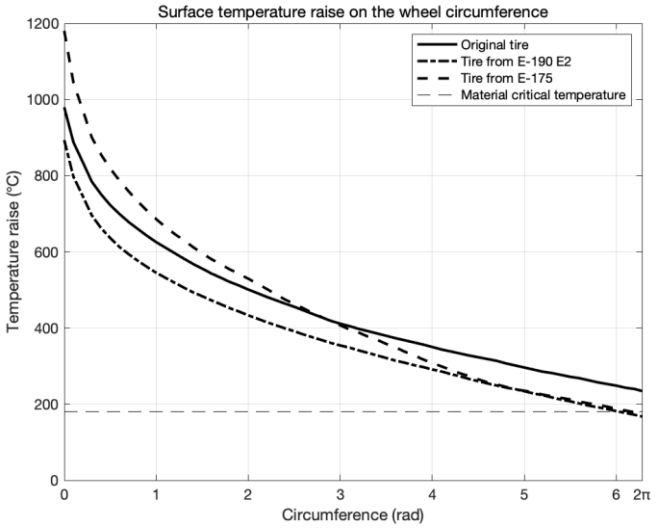

Table 10

The Friction Performance of Different Tire Options

Tire	Maximum temperature
Original E-190 tire	979.7°C
Tire from E-190 E2	893.5°C
Tire from E-175	1180.4 C

The last section tests the friction performance of various tire options on the E-190 jet. The temperature rise and friction performance are shown in Figure 11 and Table 10. First of all, if the aircraft is equipped with E-175 tires, the temperature increases significantly. Compared with the original one, the tire size of the E-175 is smaller (radius and width). Hence the contact surface area with the runway is also reduced. As a result, the energy density increases significantly when the wheel load remains unchanged. On the other hand, if the aircraft is equipped with E2 tires, the overall temperature will be significantly reduced. Such a change may benefit from the tire weight reduction under the same size. Therefore, the wheel acceleration during friction will increase (the wheel load remains unchanged), and a shorter friction time will inevitably lead

to lower heat transfer. This comparison proves the correct choice of aircraft tire and the role of new generation tire in reducing friction strength.

Conclusions

This study has established a basic MATLAB algorithm to calculate the heat generation of aircraft tire at landing. The algorithm can be further developed and commercialised to support tire design and wear reduction. Several important findings are listed as follows.

Firstly, the tire temperatures of various types of aircraft are calculated. Even though large aircraft leads to high tire temperature and material decomposition, this phenomenon also takes place on small general aviation aircraft such as DHC-6. Therefore, future research on tire wear prevention should also focus on this type of aircraft. Secondly, the influence of aircraft landing weight on tire temperature is not unique. A lower wheel load increases the friction time, causes more tire rotation and maybe more heat generation. Finally, the study compares the friction performance of different tire selections on E-190 jet. The results prove that it is possible to reduce heat generation and material loss by equipping different tires. Therefore, airlines and manufacturers may apply this algorithm to examine tire landing performance, select the most appropriate tire, and save costs.

References

Adathodi, L., Raja Murugadoss, J., & Gaddam, K. (2018). A comparative study on vehicular tyre rubber and aircraft tyre rubber: A review based on SEM eds and XRD analysis. *International Journal of Mechanical and Production Engineering Research and Development, 8*(2), 1227–1234. https://doi.org/ 10.24247/ijmperdapr2018141

Alroqi, A. A. (2017). *Investigation of the heat and wear of aircraft landing gear tyres*. (pp. 100).

Alroqi, A. A., Wang, W., & Zhao, Y. (2016). Aircraft tire temperature at touchdown with wheel prerotation. *Journal of Aircraft, 54*(3), 926–938. https://doi.org/10.2514/1.C033916

ATR. (2021). *ATR 72-600. The most fuel efficient regional aircraft.* https://www.atr-aircraft.com/our-aircraft/atr-72-600/ (Accessed: 16 April 2021).

Bennett, M., & Christie, S. M., Graham, A., Thomas, B. S., Vishnyakov, V., Morris, K., Peters, D. M., Jones, R., & Ansell, C. (2011). Composition of smoke generated by landing aircraft. *Environmental Science & Technology, 45*, 3533- 8. 10.1021/es1027585

Bhushan, B. (2013). Interface temperature of sliding surfaces. In Introduction to Tribology (p. 275). https://doi.org/10.1002/9781118403259.c h6

CAA. (2004). *Tire tread loss and airframe damage, Boeing 737-33A, 9H-ADH*.

Clark, T. (2013). *Advancements in rubber disposal: Biodegradation and the environment*. In The International Latex Conference (pp. 2–19).

Dawson, T. R., & Porritt, B. D. (1935). *Rubber physical and chemical properties.* The Research Association of British Rubber Manufacturers, Croydon, England, p. 508.

Dunlop. (2021). *Aircraft*. https://www.dunlopaircrafttyres.co.uk/aircraft/ (Accessed: 16 April 2021).

Goodyear. (2002). *Aircraft tire data book*. The Goodyear Tire & Rubber Co.

Goodyear. (2020). Aircraft tire care & maintenance. https://www.goodyearaviation.com/resources/pdf/aviati on-tire-care-2020.pdf (Accessed: 23 April 2021).

Grosch, K.A. (1969). Natural rubber in tyres. *Rubb. Res. Inst. Malaya, 22*(2), 145-164.

International Institute of Synthetic Rubber Producers. (1999). *POLYBUTADIENE properties and applications.* (pp. 1–4).

Jones, E. R., & Childers, R. L. (1993). *Contemporary college physics*. Addison-Wesley.

Keyser, J. H. (1948). Electrical prerotation of landing gear wheels. *Electrical Engineering, 67*(12), 1154-1159. doi:10.1109/EE.1948.6444490.

Kuo, W. L., & Lin, J. F. (2006). General temperature rise solution for a moving plane heat source problem in surface grinding. International *Journal of Advanced Manufacturing Technology, 31*(3–4), 268– 277. https://doi.org/10.1007/s00170-005-0200-0

Majer, V., & Svoboda, V. (1985). *Enthalpies of vaporization of organic compounds: A critical review and data compilation*. Blackwell Scientific Publications.

Merget, R., Bauer, T., Küpper, H., Philippou, S., Bauer, H., Breitstadt, R., & Bruening, T. (2002). Health hazards due to the inhalation of amorphous silica. *Archives of Toxicology*. Springer Verlag. https://doi.org/10.1007/s002040100266

Saibel, E. A., & Tsai, C. (1973). Tire wear by ablation. *Wear, 24*(24), 161–176. doi:10.1016/0043-1648(73)90229-9

Skybrary. (2021). *Aircraft*. https://www.skybrary.aero/index.php/ Category: Aircraft (Accessed: 16 April 2021).

Tsonopoulos, C., & Ambrose, D. (1996). Vapor-liquid critical properties of elements and compounds. 6. Unsaturated aliphatic hydrocarbons. *J. Chem. Eng. Data, 41*, 645-656.

Watt, S. (2017). *WINDY! Approaches into St Barts (dangerous landing!).* Available at https://www.youtube.com/watch?v=JBxpxK3MO5w (Accessed: 15 April 2021).

Zakrajsek, A. J., Childress, J., Bohun, M. H., Naboulsi, S., Vogel, R. N., Lindsey, N. J. & Mall, S. (2016). *Aircraft tire spin-up wear analysis through experimental testing and computational modeling*. In 57th AIAA/ASCE/AHS/ASC Structures, Structural Dynamics, and Materials Conference. American Institute of Aeronautics and Astronautics. https://doi.org/doi:10.2514/6.2016-0413